Research Square

Preprints are preliminary reports that have not undergone peer review. They should not be considered conclusive, used to inform clinical practice, or referenced by the media as validated information.

Atmospheric and oceanic pathways linking the Pacific–Japan pattern to summer salinity variability in the Bay of Bengal

Srinivas Gangiredla

srinivasg.nio@csir.res.in

National Institute of Oceanography CSIR

Nitesh Maury

NIO: National Institute of Oceanography CSIR

Deepti D. Nagvekar

NIO: National Institute of Oceanography CSIR

Srujitha Pothula

IITM: Indian Institute of Tropical Meteorology

Jasti S. Chowdary

IITM: Indian Institute of Tropical Meteorology

Subhra Prakash Dey

NIO: National Institute of Oceanography CSIR

Rajesh Sikhakoli

NRSC: National Remote Sensing Centre

Research Article

Keywords: Pacific – Japan pattern, Bay of Bengal, Sea Surface Salinity, Atmospheric pathways, Mixed-layer Salinity Budget, Kelvin and Rossby waves

Posted Date: October 16th, 2026

DOI: https://doi.org/10.21203/rs.3.rs-11186743/v1

License: This work is licensed under a Creative Commons Attribution 4.0 International License. Read Full License

Atmospheric and oceanic pathways linking the Pacific–Japan pattern to summer salinity variability in the Bay of Bengal

Srinivas G[1,2]*, Nitesh Maury[1,3], Deepti D. Nagvekar[1,2], Srujitha Pothula[2,4], Jasti S. Chowdary[4], Subhra Prakash Dey[1,2] and Rajesh Sikhakoli[5]

[1]CSIR-National Institute of Oceanography, Goa, India
[2]Academy of Scientific and Innovative Research, Ghaziabad, India
[3]Department of Geography, Central University of Haryana, Haryana, India
[4]Indian Institute of Tropical Meteorology, Ministry of Earth Sciences, Pune, India
[5]National Remote Sensing Center, Indian Space Research Organization, Hyderabad, India
*srinivasg.nio@csir.res.in

Abstract

The Pacific–Japan (PJ) pattern is a leading mode of boreal-summer atmospheric variability that influences Indo–Pacific hydroclimate through large-scale atmospheric teleconnections. Here, we demonstrate that the PJ pattern also exerts a significant influence on sea surface salinity (SSS) variability in the Bay of Bengal (BoB) during June–August. The positive PJ phase is associated with a pronounced meridional SSS dipole, characterized by salinification in the northern BoB and freshening farther south. This relationship persists after removing the combined influence of El Niño–Southern Oscillation and the Indian Ocean Dipole, indicating a distinct PJ influence on BoB salinity. Mixed-layer salinity-budget analysis reveals contrasting mechanisms across the basin. Horizontal advection provides the dominant resolved contribution to northern BoB salinification, whereas anomalous surface freshwater forcing associated with enhanced precipitation primarily drives southern BoB freshening. Sea-level propagation further reveals a dynamical pathway connecting remote forcing to the BoB: equatorial and coastal Kelvin-wave signals propagate toward the eastern and northern boundaries and subsequently radiate westward into the basin interior as Rossby waves, modifying sea surface height and upper-ocean circulation. Composite analyses show that the dominant salinity, rainfall, and circulation responses broadly reverse between positive and negative PJ phases, indicating an approximately linear response, while weaker asymmetric anomalies over the northern BoB point to nonlinear oceanic adjustment and phase-dependent freshwater redistribution. These results establish the PJ pattern as an important remote driver of BoB salinity variability through coupled atmospheric freshwater forcing and ocean dynamical adjustment, providing a pathway linking western North Pacific climate variability to the northern Indian Ocean.

Keywords: Pacific – Japan pattern, Bay of Bengal, Sea Surface Salinity, Atmospheric pathways, Mixed-layer Salinity Budget, Kelvin and Rossby waves.

1. Introduction

Sea surface salinity (SSS) in the Bay of Bengal (BoB) is an essential oceanographic variable that regulates upper-ocean stratification, mixed-layer dynamics, and air–sea interactions (e.g., Schmitt, 2008; Vinayachandran and Nanjundiah, 2009). The BoB exhibits one of the strongest salinity gradients in the global tropics, maintained by the combined effects of intense monsoonal precipitation, river discharge, evaporation, and ocean circulation (Delcroix et al., 2005; Yu, 2011; Gordon et al., 2016). Variations in SSS alter upper-ocean density, influencing mixed-layer depth, barrier-layer formation, and sea surface temperature (SST), thereby modulating air–sea coupling, monsoon variability, and regional climate (Lukas and Lindstrom, 1991; Sprintall and Tomczak, 1992; Rao and Sivakumar, 2003; Vinayachandran et al., 2002).

On interannual timescales, BoB salinity variability is primarily controlled by large-scale climate modes, particularly the El Niño–Southern Oscillation (ENSO) and the Indian Ocean Dipole (IOD) (Delcroix and Murtugudde, 2002; Grunseich et al., 2011). Superimposed on these basin-scale influences, regional processes including freshwater fluxes, river discharge, and horizontal advection substantially modify the salinity distribution (Akhil et al., 2016). ENSO alters the freshwater budget through changes in the Walker circulation, which reorganize atmospheric convection, moisture transport, and precipitation over the Indian Ocean. ENSO also modulates the Indonesian Throughflow, thereby controlling the transport of relatively fresh Pacific waters into the eastern Indian Ocean and influencing upper-ocean salinity (e.g., Delcroix et al., 2011; Hasson et al., 2013; Maes et al., 2014). Likewise, IOD-induced changes in surface winds and rainfall generate pronounced salinity anomalies across the equatorial and eastern Indian Ocean through modifications of freshwater fluxes and ocean circulation (Nyadjro et al., 2012; Akhil et al., 2014; Thompson et al., 2006). These salinity anomalies subsequently feed back onto the coupled ocean–atmosphere system by modifying upper-ocean stability and SST evolution, thereby influencing the predictability of Indian Ocean climate variability (Mignot et al., 2007; Durand et al., 2013).

Beyond ENSO and the IOD, the Pacific–Japan (PJ) pattern is a dominant mode of boreal-summer atmospheric variability over the western North Pacific. Through large-scale atmospheric teleconnections, the PJ pattern strongly influences the Indian summer monsoon by modulating circulation, moisture transport, and convection across the Indo-Pacific region (Nitta, 1987;

Wakabayashi and Kawamura, 2004; Kosaka and Nakamura, 2006; Srinivas et al., 2018). These atmospheric anomalies can, in turn, alter freshwater fluxes and upper-ocean salinity in the Bay of Bengal (BoB). However, Unlike ENSO and the IOD, which have been shown to exert substantial control over Indian Ocean salinity variability (Delcroix and Murtugudde, 2002; Grunseich et al., 2011; Akhil et al., 2014), the role of the PJ pattern in modulating BoB sea surface salinity (SSS) has received limited attention. The physical pathways linking PJ-related atmospheric forcing to changes in the BoB salinity remain largely unresolved.

The recent availability of satellite-derived salinity observations provides an unprecedented opportunity to quantify the large-scale salinity response to atmospheric teleconnections. In this study, we investigate the influence of the Pacific–Japan pattern on Bay of Bengal SSS variability during boreal summer (June–August) largely using the satellite datasets. We first characterize the spatial structure of PJ-induced salinity anomalies and then quantify the relative contributions of surface freshwater fluxes, horizontal salinity advection, and remote oceanic wave dynamics using mixed-layer salinity budget diagnostics. Finally, we examine the asymmetry of salinity responses between the positive and negative phases of the PJ pattern to identify the nonlinear oceanic processes governing the upper-ocean salinity adjustment. The remainder of the paper is organized as follows. Section 2 describes the datasets, methodology, and mixed-layer salinity budget analysis. Section 3 examines the response of Bay of Bengal salinity to the Pacific–Japan pattern. Section 4 investigates the asymmetry of salinity variability during the positive and negative PJ phases. Finally, Section 5 summarizes the principal findings and discusses their broader implications.

2. Datasets and Methods

2.1. Datasets

Satellite Products

Satellite-derived sea surface salinity (SSS) is obtained from the Multi-Observation Global Ocean Sea Surface Salinity and Sea Surface Density dataset (Product ID: MULTIOBS_GLO_PHY_S_SURFACE_MYNRT_015_013) distributed by the Copernicus Marine Environment Monitoring Service (CMEMS) for the period 2005–2025 (Droghei et al.,

2016). Surface winds obtain from the Level-3 scatterometer bias-corrected CMEMS Global Ocean Monthly Mean Sea Surface Wind and Stress dataset (WIND_GLO_PHY_CLIMATE_L4_MY_012_003) (Belmonte Rivas and Stoffelen, 2019). Surface currents are derived from the National Information System for Climate and Environment Studies (NICES) product (Sikhakolli et al., 2013), which combines a diagnostic surface-current model with Cross-Calibrated Multi-Platform (CCMP) surface winds (Mears et al., 2022). Sea surface height (SSH) is obtained from the AVISO multi-mission satellite altimeter product (Pujol et al., 2016), while monthly precipitation is taken from the Global Precipitation Climatology Project (GPCP), which merges observations from multiple satellite platforms to provide a consistent estimate of global precipitation (Adler et al., 2003).

Reanalysis and In-situ datasets

The three-dimensional oceanic response associated with the PJ pattern is examined using the European Centre for Medium-Range Weather Forecasts (ECMWF) Ocean Reanalysis System 5 (ORAS5; Zuo et al., 2019). ORAS5 provides monthly temperature, salinity, ocean current, and sea surface height fields at a horizontal resolution of 0.25° × 0.25° for the period 1980–2025. The reanalysis assimilates diverse observational datasets, including Argo profiles, satellite measurements, and conventional in situ observations, thereby providing a dynamically consistent representation of upper-ocean variability. Monthly zonal and meridional winds at 850 hPa are obtained from ECMWF Reanalysis (ERA5) (Hersbach et al., 2020) to compute relative vorticity over the western North Pacific (WNP). In addition to these reanalysis and satellite products, we also utilize the in-situ measured gridded Argo salinity observations (Jean-Michel et al. 2021) and EN4 objective analyses datasets (Wong et al. 2020).

2.2 Methods

Statistical analyses: Identification of PJ events

The PJ pattern is extracted using empirical orthogonal function (EOF) analysis of JJA mean 850-hPa relative vorticity anomalies over the WNP, following Kosaka et al. (2013) and Srinivas et al. (2018, 2024). The leading EOF mode (EOF1), which characterizes the PJ pattern, explains approximately 16% of the total variance. The influence of the PJ pattern on the salinity variability

is examined using regression, correlation, and composite analyses. Unless otherwise stated, statistical significance is evaluated using a two-tailed Student's *t*-test at the 95% confidence level.

Mixed-Layer Salinity Budget

The relative contributions of atmospheric forcing and oceanic processes to mixed-layer salinity (MLS) variability are quantified using the mixed-layer salinity budget formulation of Vialard and Delecluse (1998) and Jain et al. (2021). To ensure consistency in the budget calculations, the mixed-layer depth (MLD) is extended to the base of the corresponding model grid cell. The tendency of the vertically averaged mixed-layer salinity is expressed as

$$\partial_t S_{ML} = \underbrace{\frac{[S_0(E-P)]}{h}}_{Atmospheric\ forcing} + \underbrace{\frac{-1}{h}\left(\int_{-h}^{0} u\partial_x S\, dz + \int_{-h}^{0} v\partial_y S\, dz\right)}_{Horizontal\ advection} + \underbrace{\frac{1}{h}[w_{-h}(S_{-h} - S_{ML})]}_{Vertical\ advection}$$

$$+ \underbrace{\frac{1}{h}[H(\partial_t h)\,(S_{-h} - S_{ML}) + (K\partial_z S)_{-h}]}_{Entrainment} + \underbrace{R}_{Residual}$$

Here, (S) denotes salinity, (S_o) the surface salinity, (S_{ML}) the mixed-layer mean salinity. The residual is computed as the difference between the total salinity tendency and the sum of all explicitly estimated budget terms, thereby accounting for unresolved physical processes, numerical truncation errors, and uncertainties associated with the budget calculation. The salinity and MLD datasets are considered from the multi-observational 3D fields of the Copernicus dataset, zonal and meridional currents from ORAS5, and rainfall and evaporation variables considered from the ERA5.

3. Bay of Bengal salinity response to Pacific-Japan pattern

The leading mode of JJA 850-hPa relative vorticity variability over the WNP exhibits the characteristic spatial structure of the PJ pattern (Fig. 1a). The corresponding standardized principal component (PC1), hereafter referred to as the PJ index, shows pronounced interannual variability during the analysis period (Fig. 1b). Positive (1983, 1988, 1996, 1998, 2008, 2010, 2020, 2022, 2023) and negative (1990, 1994, 1997, 2001, 2002, 2004, 2009, 2018) PJ events are identified when the standardized index exceeds ±1 standard deviation, respectively (Fig. 1b). The PJ pattern is significantly associated with SSS variability over the Bay of Bengal. Correlation of the PJ index

with JJA SSS reveals a pronounced meridional dipole, characterized by positive correlations over the northern and northeastern BoB and negative correlations over the central and southern basin (Fig. 1c). Thus, the positive PJ phase is associated with anomalously saline conditions in the northern BoB and fresher conditions farther south. The strongest and most spatially coherent relationship occurs over the northern BoB, where correlations exceed 0.6 over a broad region. Because both ENSO and the IOD can influence tropical Indian Ocean hydroclimate and salinity (e.g., Phillips et al. 2021; Hu et al. 2025), their contribution to the PJ–SSS relationship is examined using partial correlation. After removing the combined influence of ENSO and IOD, the characteristic meridional SSS pattern remains evident, with positive correlations persisting over the northern BoB and negative correlations over the central and southwestern basin (Fig. 1d). Although the magnitude and spatial extent of the correlations are somewhat reduced, particularly over the northern BoB, the persistence of the dipole indicates that the PJ–SSS relationship cannot be explained solely by concurrent ENSO and IOD variability. This provides evidence for an independent contribution of PJ-related atmospheric variability to interannual BoB salinity variability.

The robustness of the PJ-related salinity response is further evaluated using four independent salinity products, including gridded Argo observations, EN4 objective analyses, and the ORAS5 and GLORYS Ocean reanalyses (Fig. 2). All products reproduce the broad meridional contrast identified in the satellite observations, demonstrating that the relationship is not dependent on a particular dataset. Differences are most evident over the northern BoB, particularly among the reanalysis products, and likely reflect differences in the representation of river discharge, surface freshwater fluxes, vertical mixing, and coastal processes (e.g., Akhil et al., 2020). Nevertheless, the overall agreement among independent products supports the robustness of the PJ-related BoB salinity signal.

To identify the processes underlying this response, Fig. 3 presents regressions of SSS, precipitation, sea surface height (SSH), surface currents, and winds onto the PJ index. The meridional SSS dipole is accompanied by pronounced atmospheric and oceanic anomalies. Positive PJ conditions are associated with suppressed precipitation over the northern and northeastern BoB and enhanced rainfall over the southern BoB and equatorial eastern Indian Ocean (Fig. 3b). The PJ teleconnection modifies the summer monsoon circulation through the

development of an anomalous anticyclone over the northern Indian Ocean (Srinivas et al., 2018; Kosaka et al., 2021). Concurrently, anomalous surface winds extend across the central and northern BoB (Fig. 3d), while predominantly positive SSH anomalies and associated circulation changes occur over much of the northern and central basin (Fig. 3c). The spatial correspondence among SSS, precipitation, SSH, and circulation anomalies indicates that the PJ-related salinity response involves both anomalous surface freshwater forcing and dynamically driven redistribution of upper-ocean freshwater.

The mixed-layer salinity budget further distinguishes these contributions (Fig. 4). Positive salinity tendencies dominate parts of the northern and northeastern BoB, whereas negative tendencies occur over much of the central and southern basin (Fig. 4a), broadly consistent with the SSS response. Surface freshwater forcing contributes to this meridional contrast, with positive anomalies over parts of the northern and northeastern BoB and predominantly negative anomalies farther south (Fig. 4b). The latter are consistent with enhanced precipitation during the positive PJ phase (Fig. 3b). Horizontal advection exhibits stronger spatial heterogeneity, with pronounced positive and negative contributions concentrated near the northern boundary and in regions of strong background salinity gradients (Fig. 4c). The residual remains appreciable in several regions (Fig. 4d), suggesting contributions from unresolved vertical processes and mixing, as well as uncertainties associated with combining observational and reanalysis products.

The regional budget provides a clearer quantitative assessment of the processes controlling the salinity dipole (Fig. 5). The northern BoB exhibits a positive salinity tendency of approximately 0.08, whereas the southern BoB shows a negative tendency of approximately −0.06, confirming the contrasting responses evident in the spatial regression. Importantly, the processes responsible for these tendencies differ markedly between the two regions. In the northern BoB, horizontal advection (~0.06) constitutes the largest resolved positive contribution, while vertical advection provides only a small positive contribution. Entrainment (~−0.02) and the residual (~−0.03) oppose the salinification. Thus, although reduced precipitation locally favors increased salinity over parts of the northern BoB, the regional budget indicates that anomalous horizontal salinity transport is the dominant resolved mechanism supporting the area-averaged positive salinity tendency. The southern BoB exhibits a fundamentally different balance. Surface freshwater forcing (~−0.04) provides the largest contribution to the negative salinity tendency,

consistent with enhanced precipitation over the southern BoB and equatorial eastern Indian Ocean during the positive PJ phase. Horizontal advection provides a smaller negative contribution (~−0.01), while vertical advection and entrainment are comparatively weak. The regional budget therefore reveals a clear mechanistic contrast: northern BoB salinification is predominantly associated with anomalous horizontal advection, whereas surface freshwater forcing primarily controls southern BoB freshening.

The dominance of horizontal advection in the northern BoB raises the question of how PJ-related atmospheric forcing generates the circulation anomalies required to redistribute freshwater. To address this, the oceanic adjustment is examined using PJ-regressed sea-level anomalies (SLA) along the equatorial–coastal waveguide and across the BoB interior (Fig. 6). The pathway–time analysis shows coherent SLA anomalies evolving along the equatorial and coastal boundaries during boreal summer (Fig. 6a–b). Positive SLA anomalies are prominent along the initial sections of the pathway during June and subsequently extend toward the eastern and northern BoB, consistent with the propagation of downwelling equatorial and coastal Kelvin-wave signals. The lag–distance regression provides additional evidence for this propagating response (Fig. 6c). Coherent SLA anomalies progress over several thousand kilometres along the pathway and evolve over subsequent weeks, indicating that the sea-level response is not spatially simultaneous but contains a distinct propagating component. Upon reaching the eastern boundary of the BoB, part of the coastal disturbance radiates into the basin interior. Along 14°N, coherent SLA anomalies display a pronounced westward displacement from the eastern and central BoB toward the western basin during June–July (Fig. 6d), consistent with westward-propagating Rossby waves. Such Kelvin-to-Rossby wave adjustment provides an established mechanism for transmitting remotely generated sea-level disturbances from the equatorial Indian Ocean and eastern boundary into the northern Indian Ocean interior (McCreary et al., 1993; Clarke and Liu, 1994; Shankar et al., 2002).

This wave adjustment provides a dynamical framework for interpreting the SSH, circulation, and salinity-budget responses. The positive SSH anomalies over the northern and central BoB (Fig. 3c) are consistent with the downwelling wave signals identified in Fig. 6. As these disturbances propagate along the boundary and subsequently westward into the basin, they alter upper-ocean pressure gradients and circulation, thereby modulating horizontal freshwater transport. This connection is particularly relevant to the northern BoB, where strong background

salinity gradients make SSS highly sensitive to circulation changes and where the regional budget identifies horizontal advection as the dominant resolved salinifying process (Figs. 4c and 5). The wave response therefore provides a plausible dynamical pathway through which PJ-related remote forcing reorganizes upper-ocean circulation and freshwater distribution rather than directly generating the salinity anomalies.

Overall, this section establish a coherent pathway linking WNP atmospheric variability to BoB salinity. The persistence of the PJ–SSS relationship after removing the influence of ENSO and IOD demonstrates that the connection is not simply a manifestation of these dominant tropical climate modes (Fig. 1). During the positive PJ phase, atmospheric circulation anomalies modify precipitation and surface winds over the tropical Indian Ocean (Fig. 3), while the associated oceanic adjustment is communicated through equatorial and coastal Kelvin waves and subsequently into the BoB interior through westward-propagating Rossby waves (Fig. 6). These circulation changes enhance horizontal salinity advection in the northern BoB, where dynamical freshwater redistribution provides the dominant resolved positive contribution to the salinity tendency. In contrast, enhanced precipitation and associated surface freshwater forcing dominate the freshening response in the southern BoB. The PJ-related SSS dipole therefore emerges from the spatially contrasting influence of ocean dynamical redistribution in the northern BoB and atmospheric freshwater forcing in the southern BoB, establishing a pathway through which WNP climate variability influences upper-ocean salinity in the northern Indian Ocean.

4. BoB salinity symmetric and asymmetric response to PJ pattern

Regression and mixed-layer salinity-budget analyses establish a robust relationship between the PJ pattern and BoB salinity variability, but do not reveal whether the oceanic response is symmetric between positive and negative PJ phases. To examine this phase dependence, composite analyses are performed using ORAS5 and ERA5 for 1980–2025, extending the assessment beyond the satellite SSS period. Figure 7 shows composite anomalies of SSS, SSH and surface currents, precipitation, and surface winds during positive and negative PJ events. During the positive PJ phase, a pronounced meridional salinity contrast develops over the BoB, with positive SSS anomalies concentrated in the northern basin and predominantly negative anomalies over the central and southern BoB (Fig. 7a). This pattern closely resembles the PJ-regressed SSS response

(Fig. 3a), despite differences in datasets and analysis periods. The northern salinification is accompanied by suppressed precipitation (Fig. 7c), positive SSH anomalies, and anomalous circulation over the northern BoB (Fig. 7b). Enhanced rainfall farther south coincides with negative SSS anomalies, consistent with the dominant contribution of surface freshwater forcing to southern BoB freshening identified from the mixed-layer salinity budget (Figs. 4 and 5). Over the northern BoB, however, the budget analysis shows that horizontal advection provides the largest resolved positive contribution to the salinity tendency. The SSH and current anomalies in the positive PJ composite therefore support an important role for circulation-driven redistribution of freshwater in maintaining the northern salinity anomaly. The response broadly reverses during the negative PJ phase (Fig. 7d–f). Negative SSS anomalies dominate the northernmost BoB, accompanied by negative SSH anomalies and enhanced precipitation, whereas positive SSS anomalies occur over parts of the southern and eastern basin (Fig. 7d–f). The reversal of the large-scale SSS, SSH, and rainfall patterns indicates that a substantial fraction of the BoB response varies approximately linearly with the sign of the PJ forcing. However, the amplitudes and spatial structures of the positive and negative composites are not exact mirror images. In particular, the northern BoB exhibits differences in the location and magnitude of the SSS and SSH anomalies between the two phases, suggesting a degree of nonlinear oceanic adjustment.

To isolate these components, the positive and negative PJ composites are decomposed into symmetric and asymmetric responses (Fig. 8). The symmetric component, obtained from the difference between the positive and negative composites, captures the portion of the response that reverses sign with the PJ phase. It reproduces the dominant meridional SSS structure, with strong positive anomalies over the northern BoB and negative anomalies over much of the central and southern basin (Fig. 8a). The corresponding fields show predominantly positive SSH anomalies over the northern and central BoB (Fig. 8b), together with suppressed precipitation over the northern and northeastern basin and enhanced precipitation farther south (Fig. 8c). The close correspondence between the symmetric SSS, SSH, circulation, and rainfall anomalies demonstrates that the leading BoB response is approximately linear with respect to PJ forcing.

In contrast, the asymmetric component, obtained from the sum of the positive and negative composites, represents anomalies that do not reverse sign between the two PJ phases (Fig. 8d–f). Its amplitude is generally weaker than that of the symmetric component, but substantial SSS

anomalies remain over the northern BoB, particularly near the northern boundary and western sector (Fig. 8d). The corresponding SSH and current anomalies are also concentrated primarily in the northern basin (Fig. 8e), whereas the rainfall and wind asymmetries are comparatively weaker and spatially less coherent (Fig. 8f). This contrast suggests that solely asymmetric atmospheric freshwater forcing and points to a greater contribution from nonlinear ocean dynamical processes cannot explain the asymmetry in the salinity response.

The concentration of the asymmetric SSS and SSH signals in the northern BoB is particularly relevant because this region is characterized by strong background salinity gradients and a dominant contribution from horizontal advection to the PJ-related salinity tendency (Figs. 4 and 5). Relatively small differences in circulation between positive and negative PJ phases can therefore produce substantial differences in horizontal freshwater transport. The Kelvin–Rossby wave adjustment identified from the SLA propagation analysis (Fig. 6) provides a dynamical context for this behaviour: remotely forced wave signals modify SSH and upper-ocean pressure gradients, while their interaction with the background circulation and strong salinity gradients can produce phase-dependent freshwater redistribution. Thus, the weaker asymmetric component is consistent with nonlinear oceanic adjustment superimposed on the dominant linear response to PJ forcing.

Overall, the composite and symmetric–asymmetric analyses demonstrate that the BoB salinity response to the PJ pattern consists of a dominant approximately linear component and a weaker nonlinear component. The linear response is characterized by a meridional SSS contrast accompanied by coherent rainfall, SSH, wind, and circulation anomalies that broadly reverse between positive and negative PJ phases. Within this response, surface freshwater forcing plays the leading role in southern BoB freshening, whereas horizontal advection is the dominant resolved contribution to northern BoB salinification. The weaker asymmetric response is concentrated primarily over the northern BoB and is more clearly expressed in SSS and SSH than in the atmospheric fields, indicating an enhanced role for nonlinear ocean dynamics and phase-dependent freshwater redistribution. Together with the wave diagnostics, these results show that PJ-related BoB salinity variability reflects the combined effects of atmospheric freshwater forcing, remotely forced oceanic adjustment, and regional horizontal salinity transport.

5. Summary and conclusions

This study demonstrates that the Pacific–Japan (PJ) pattern is an important driver of boreal summer sea surface salinity (SSS) variability in the Bay of Bengal (BoB). Using satellite observations, independent in situ products, and ocean reanalyses, we identify a robust atmospheric–oceanic teleconnection linking western North Pacific (WNP) atmospheric variability to upper-ocean salinity changes across the northern Indian Ocean. The PJ pattern produces a pronounced meridional salinity dipole over the BoB, characterized by positive SSS anomalies in the northern basin and negative anomalies in the southern basin, while weaker but spatially coherent salinity anomalies also extend into the Arabian Sea (Figure not shown). The consistency of these signals across multiple observational and reanalysis products demonstrates that the PJ-related salinity response is a robust feature of the Indo-Pacific climate system.

The physical mechanisms underlying this teleconnection are summarized schematically in Figure 9. During the positive PJ phase, the anomalous anticyclonic circulation over the western North Pacific modifies the climatological summer monsoon circulation, altering moisture transport, precipitation, and evaporation across the Bay of Bengal (Nitta, 1987; Kosaka and Nakamura, 2006; Srinivas et al., 2018). Suppressed precipitation together with enhanced evaporation over the northern BoB increases surface salinity, whereas enhanced precipitation over the southern BoB produces widespread freshening. Concurrently, the anomalous wind forcing excites coastal Kelvin waves along the eastern boundary of the Bay of Bengal and the Maritime Continent, which subsequently radiate westward into the basin interior as downwelling Rossby waves (Clarke and Liu, 1994; McCreary et al., 1993; Shankar et al., 2002). These remotely forced oceanic waves reorganize sea surface height and upper-ocean circulation, thereby redistributing salinity anomalies throughout the basin. Mixed-layer salinity budget analysis further demonstrates that freshwater-flux anomalies associated with evaporation minus precipitation (E–P) constitute the primary driver of the PJ-induced salinity response, whereas horizontal advection and upper-ocean mixing regulate the redistribution and amplification of these anomalies. The symmetric–asymmetric decomposition reveals that the BoB salinity dipole, associated rainfall anomalies, and large-scale circulation changes primarily represent a linear response to PJ forcing. In contrast, the weaker asymmetric component arises from nonlinear ocean dynamical adjustments associated with coastal Kelvin waves, Rossby-wave propagation, and upper-ocean circulation changes, which

modulate the magnitude and spatial distribution of the salinity response. These results indicate that atmospheric forcing establishes the dominant salinity signal, while ocean dynamics determine its spatial evolution and persistence.

Overall, this study identifies a previously unrecognized atmospheric–oceanic pathway through which the Pacific–Japan pattern modulates Bay of Bengal salinity variability. By linking western North Pacific atmospheric variability to freshwater fluxes, upper-ocean circulation, and salinity stratification in the Bay of Bengal, this work advances our understanding of Indo-Pacific climate interactions and their influence on upper-ocean hydrography. Because upper-ocean salinity strongly regulates mixed-layer stability, barrier-layer formation, and air–sea coupling (Sprintall and Tomczak, 1992; Schmitt, 2008; Vinayachandran and Nanjundiah, 2009), the PJ-related salinity variability identified here has important implications for seasonal prediction of the Indian summer monsoon, tropical Indian Ocean climate variability, and coupled ocean–atmosphere predictability. Future work should assess the representation of this newly identified PJ–Indian Ocean salinity teleconnection in coupled climate models and evaluate its influence on seasonal prediction and future climate projections under anthropogenic warming.

Acknowledgements

The authors thank the Director, CSIR-National Institute of Oceanography (NIO) for providing necessary computational facilities. Deepti Nagvekar acknowledge the support and data/fellowship provided by the National Information System for Climate and Environment Studies (NICES) program of the Indian Space Research Organization (ISRO) and the National Remote Sensing Centre (NRSC). Python and Ferret (PMEL/NOAA) are used for analysis and graphics. This is CSIR-NIO contribution xxxx.

Data availability

The Ssalto/Duacs altimeter products were produced and distributed by the Copernicus Marine and Environment Monitoring Service (CMEMS) (http://marine.copernicus.eu). CMEMS ARMOR3D products can be downloaded from http://marine.copernicus.eu/services-portfolio/access-to-products/. NICES currents data is accessible publicly through the (https://nices.nrsc.gov.in/) and ISRO's Bhuvan platform. Multi Observation Global Ocean Sea

Surface Salinity and Sea Surface Density data is available from (https://data.marine.copernicus.eu/product/MULTIOBS_GLO_PHY_S_SURFACE_MYNRT_015_013/services). The ORAS5/ERA5 dataset is produced by ECMWF and funded by the Copernicus Climate Change Service (https://cds.climate.copernicus.eu/) and the scrips are with the corresponding author available upon valid request.

Author contributions

All authors contributed to writing—review and editing of the manuscript. Nitesh Maury and Deepti D. Nagvekar carried out conceptualization, methodology, data collection, formal analysis, and visualization. Srinivas G wrote the first draft of the manuscript, and all authors provided comments on previous versions of the manuscript. Srinivas G. supervised the study. All authors read and approved the final manuscript.

Funding sources

The National Information System for Climate and Environment Studies (NICES) program of the Indian Space Research Organisation (ISRO) and the National Remote Sensing Centre (NRSC) supported this research.

Declaration of competing interest

The authors declare that they have no known competing financial interests or personal relationships that could have appeared to influence the work reported in this paper.

References

Adler RF, Huffman GJ, Chang A, Ferraro R, Xie PP, Janowiak J, Nelkin E (2003) The version-2 global precipitation climatology project (GPCP) monthly precipitation analysis (1979–present). J Hydrometeorol 4:1147–1167

Akhil VP, Durand F, Lengaigne M, Vialard J, Keerthi MG, Gopalakrishna VV, de Boyer Montégut C (2014) A modeling study of the processes of surface salinity seasonal cycle in the Bay of Bengal. J Geophys Res Oceans 119:3926–3947

Akhil VP, Lengaigne M, Vialard J, Durand F, Keerthi MG, Chaitanya AVS, de Boyer Montégut C (2016) A modeling study of processes controlling the Bay of Bengal sea surface salinity interannual variability. J Geophys Res Oceans 121:8471–8495

Akhil VP, Vialard J, Lengaigne M, Keerthi MG, Boutin J, Vergely JL, Papa F (2020) Bay of Bengal sea surface salinity variability using a decade of improved SMOS re-processing. Remote Sens Environ 248:111964

Belmonte Rivas M, Stoffelen A (2019) Characterizing ERA-Interim and ERA5 surface wind biases using ASCAT. Ocean Sci 15:831–852

Clarke AJ, Liu X (1994) Interannual sea level in the northern and eastern Indian Ocean. J Phys Oceanogr 24:1224–1235

Delcroix T, Murtugudde R (2002) Sea surface salinity changes in the East China Sea during 1997–2001: influence of the Yangtze River. J Geophys Res Oceans 107:SRF 9-1–SRF 9-11

Delcroix T, McPhaden MJ, Dessier A, Gouriou Y (2005) Time and space scales for sea surface salinity in the tropical oceans. Deep-Sea Res I 52:787–813

Delcroix T, Alory G, Cravatte S, Corrège T, McPhaden MJ (2011) A gridded sea surface salinity data set for the tropical Pacific with sample applications (1950–2008). Deep-Sea Res I 58:38–48

Droghei R, Buongiorno Nardelli B, Santoleri R (2018) A new global sea surface salinity and density dataset from multivariate observations (1993–2016). Front Mar Sci 5:84

Durand F, Alory G, Dussin R, Reul N (2013) SMOS reveals the signature of Indian Ocean Dipole events. Ocean Dyn 63:1203–1212

Good SA, Martin MJ, Rayner NA (2013) EN4: quality controlled ocean temperature and salinity profiles and monthly objective analyses with uncertainty estimates. J Geophys Res Oceans 118:6704–6716

Gordon AL, Shroyer EL, Mahadevan A, Sengupta D, Freilich M (2016) Bay of Bengal: 2013 northeast monsoon upper-ocean circulation. Oceanography 29:82–91

Grunseich G, Subrahmanyam B, Murty VSN, Giese BS (2011) Sea surface salinity variability during the Indian Ocean Dipole and ENSO events in the tropical Indian Ocean. J Geophys Res Oceans 116:C11013

Hasson AE, Delcroix T, Dussin R (2013) An assessment of the mixed layer salinity budget in the tropical Pacific Ocean. Observations and modelling (1990–2009). Ocean Dyn 63:179–194

Hersbach H, Bell B, Berrisford P, Hirahara S, Horányi A, Muñoz-Sabater J et al (2020) The ERA5 global reanalysis. Q J R Meteorol Soc 146:1999–2049

Hu Q, Chen X, He X, Bai Y, Jiang T, Huan Y, Liang Z (2025) Impacts of IOD and ENSO on the phytoplankton's vertical variability in the Northern Indian Ocean. Front Mar Sci 12:1523434. https://doi.org/10.3389/fmars.2025.1523434

Jain V, Amol P, Aparna SG, Fernando V, Kankonkar A, Murty VSN et al (2021) Two decades of current observations in the equatorial Indian Ocean. J Earth Syst Sci 130:75

Jean-Michel L, Eric G, Romain BB, Gilles G, Angélique M, Marie D et al (2021) The Copernicus global 1/12° oceanic and sea ice GLORYS12 reanalysis. Front Earth Sci 9:698876

Kosaka Y, Nakamura H (2006) Structure and dynamics of the summertime Pacific–Japan teleconnection pattern. Q J R Meteorol Soc 132:2009–2030

Kosaka Y, Xie SP, Lau NC, Vecchi GA (2013) Origin of seasonal predictability for summer climate over the Northwestern Pacific. Proc Natl Acad Sci USA 110:7574–7579

Kosaka Y, Takaya Y, Kamae Y (2021) The Indo-western Pacific Ocean capacitor effect. In: Tropical and extratropical air-sea interactions, pp 141–169

Lukas R, Lindstrom E (1991) The mixed layer of the western equatorial Pacific Ocean. J Geophys Res Oceans 96:3343–3357

Maes C, O'Kane TJ (2014) Seasonal variations of the upper ocean salinity stratification in the Tropics. J Geophys Res Oceans 119:1706–1722

McCreary JP Jr, Kundu PK, Molinari RL (1993) A numerical investigation of dynamics, thermodynamics and mixed-layer processes in the Indian Ocean. Prog Oceanogr 31:181–244

Mears C, Lee T, Ricciardulli L, Wang X, Wentz F (2022) Improving the accuracy of the cross-calibrated multi-platform (CCMP) ocean vector winds. Remote Sens 14:4230

Mignot J, de Boyer Montégut C, Lazar A, Cravatte S (2007) Control of salinity on the mixed layer depth in the world ocean: 2. Tropical areas. J Geophys Res Oceans 112:C10010

Nitta T (1987) Convective activities in the tropical western Pacific and their impact on the Northern Hemisphere summer circulation. J Meteorol Soc Jpn 65:373–390

Nyadjro ES, Subrahmanyam B, Murty VSN, Shriver JF (2012) The role of salinity on the dynamics of the Arabian Sea mini warm pool. J Geophys Res Oceans 117:C09002

Phillips HE, Tandon A, Furue R, Hood R, Ummenhofer CC, Benthuysen JA et al (2021) Progress in understanding of Indian Ocean circulation, variability, air–sea exchange, and impacts on biogeochemistry. Ocean Sci 17:1677–1751. https://doi.org/10.5194/os-17-1677-2021

Pujol MI, Faugère Y, Taburet G, Dupuy S, Pelloquin C, Ablain M, Picot N (2016) DUACS DT2014: the new multi-mission altimeter data set reprocessed over 20 years. Ocean Sci 12:1067–1090

Rao RR, Sivakumar R (2003) Seasonal variability of sea surface salinity and salt budget of the mixed layer of the north Indian Ocean. J Geophys Res Oceans 108:3009

Schmitt RW (2008) Salinity and the global water cycle. Oceanography 21:12–19

Schott FA, Xie SP, McCreary JP Jr (2009) Indian Ocean circulation and climate variability. Rev Geophys 47:RG1002

Shankar D, Vinayachandran PN, Unnikrishnan AS (2002) The monsoon currents in the north Indian Ocean. Prog Oceanogr 52:63–120

Sikhakolli R, Sharma R, Basu S, Gohil BS, Sarkar A, Prasad KVSR (2013) Evaluation of OSCAR ocean surface current product in the tropical Indian Ocean using in situ data. J Earth Syst Sci 122:187–199

Sprintall J, Tomczak M (1992) Evidence of the barrier layer in the surface layer of the tropics. J Geophys Res Oceans 97:7305–7316

Srinivas G, Chowdary JS, Kosaka Y, Gnanaseelan C, Parekh A, Prasad KVSR (2018) Influence of the Pacific–Japan pattern on Indian summer monsoon rainfall. J Clim 31:3943–3958

Srinivas G, Vialard J, Lengaigne M, Izumo T, Guilyardi E (2022) Relative contributions of sea surface temperature and atmospheric nonlinearities to ENSO asymmetrical rainfall response. J Clim 35:3725–3745

Srinivas G, Remya PG, Dey SP, Chowdary JS, Kumar P (2024) Impact of the Pacific-Japan pattern on the tropical Indo-western Pacific Ocean surface waves. Clim Dyn 62:8729–8740

Thompson B, Gnanaseelan C, Salvekar PS (2006) Variability in the Indian Ocean circulation and salinity and its impact on SST anomalies during dipole events. J Mar Res 64

Vialard J, Delecluse P (1998) An OGCM study for the TOGA decade. Part I: role of salinity in the physics of the western Pacific fresh pool. J Phys Oceanogr 28:1071–1088

Vinayachandran PN, Murty VSN, Ramesh Babu V (2002) Observations of barrier layer formation in the Bay of Bengal during summer monsoon. J Geophys Res Oceans 107:SRF 19-1–SRF 19-9

Vinayachandran PN, Nanjundiah RS (2009) Indian Ocean sea surface salinity variations in a coupled model. Clim Dyn 33:245–263

Vinayachandran PN, Matthews AJ, Kumar KV, Sanchez-Franks A, Thushara V, George J, Joshi M (2018) BoBBLE: ocean–atmosphere interaction and its impact on the South Asian monsoon. Bull Am Meteorol Soc 99:1569–1587

Wakabayashi S, Kawamura R (2004) Extraction of major teleconnection patterns possibly associated with the anomalous summer climate in Japan. J Meteorol Soc Jpn 82:1577–1588

Wong AP, Wijffels SE, Riser SC, Pouliquen S, Hosoda S, Roemmich D et al (2020) Argo data 1999–2019: two million temperature-salinity profiles and subsurface velocity observations from a global array of profiling floats. Front Mar Sci 7:700

Yu L (2011) A global relationship between the ocean water cycle and near-surface salinity. J Geophys Res Oceans 116:C10025

Zuo H, Balmaseda MA, Tietsche S, Mogensen K, Mayer M (2019) The ECMWF operational ensemble reanalysis–analysis system for ocean and sea ice: a description of the system and assessment. Ocean Sci 15:779–808

Figures

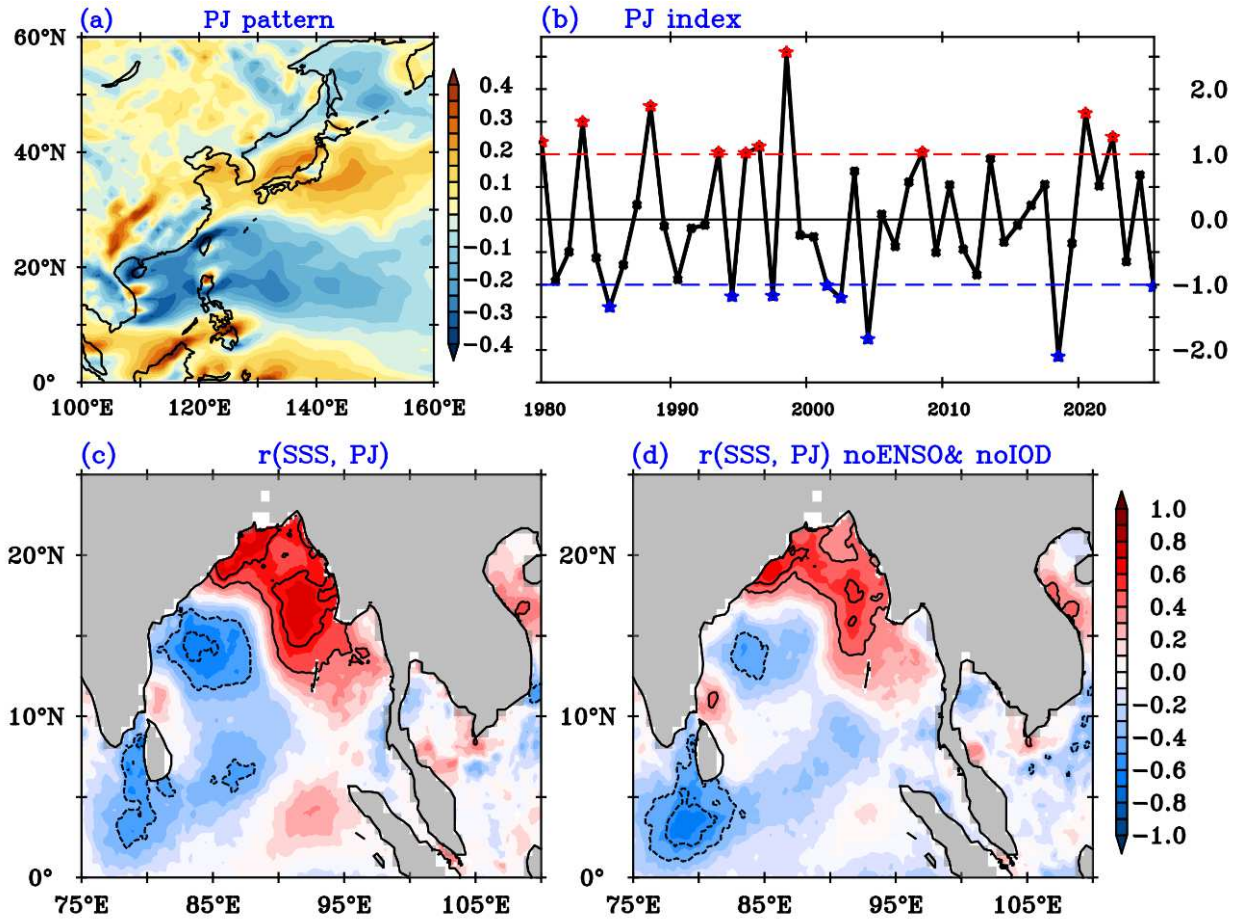

Figure 1. (**a**) Leading empirical orthogonal function (EOF1) of JJA 850-hPa relative vorticity anomalies (10^{-5} s^{-1}) over the western North Pacific. (**b**), Corresponding standardized principal component (PJ index), with positive and negative PJ years exceeding ±1 standard deviation indicated by red and blue stars, respectively. (**c**), Correlation between the PJ index and JJA sea surface salinity (SSS) anomalies. (**d**), Partial correlation between the PJ index and SSS after removing the combined influence of ENSO and the Indian Ocean Dipole (IOD). Stippling indicates statistical significance at the 95% confidence level.

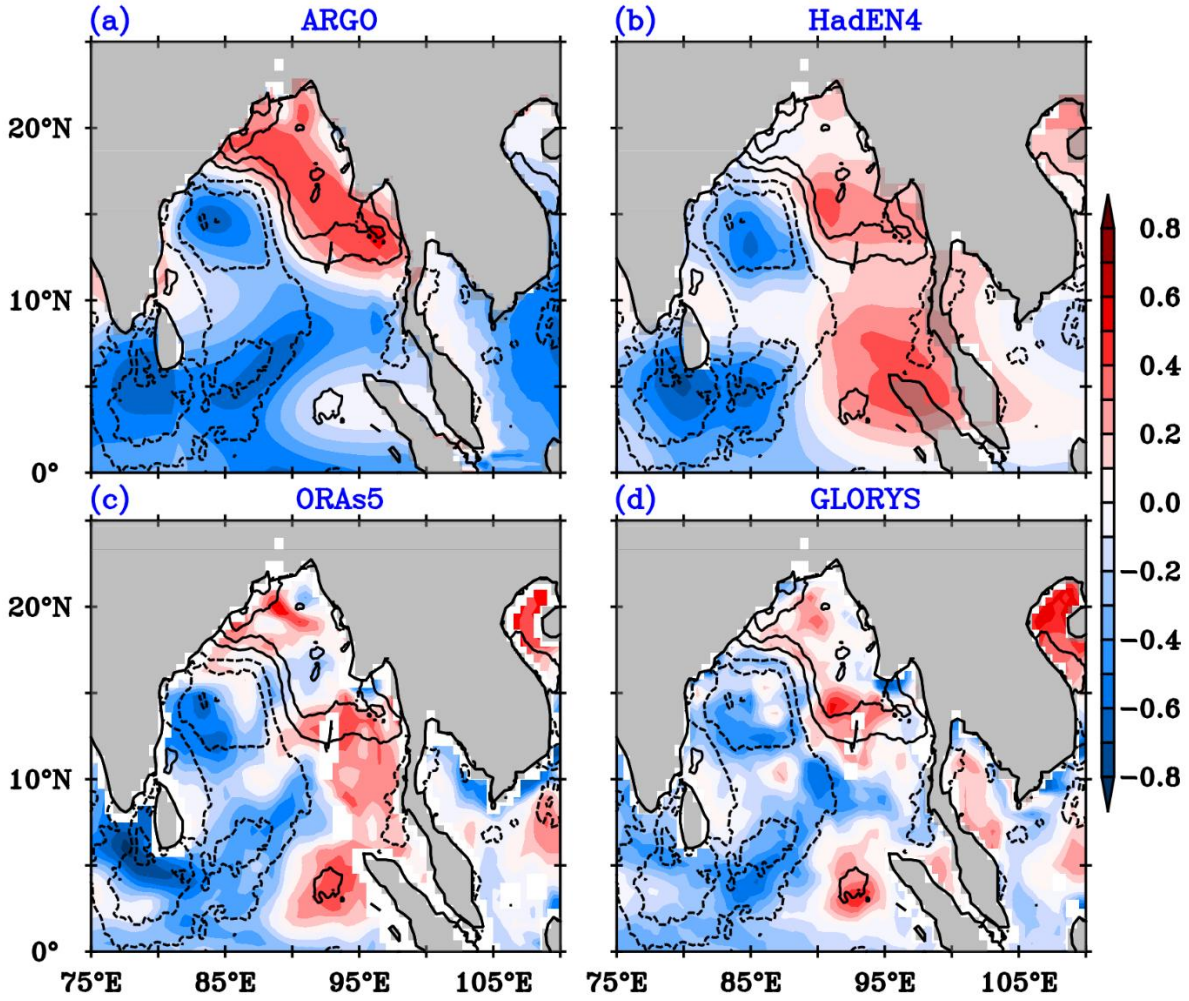

Figure 2. Correlation of PJ index with the JJA mean of SSS from different products **(a)** ARGO, **(b)** HadEN4, **(c)** ORAs5 and **(d)** GLORYS datasets. Contours on all the panels show the correlation of PJ with satellite salinity measurements, same as figure **1d**.

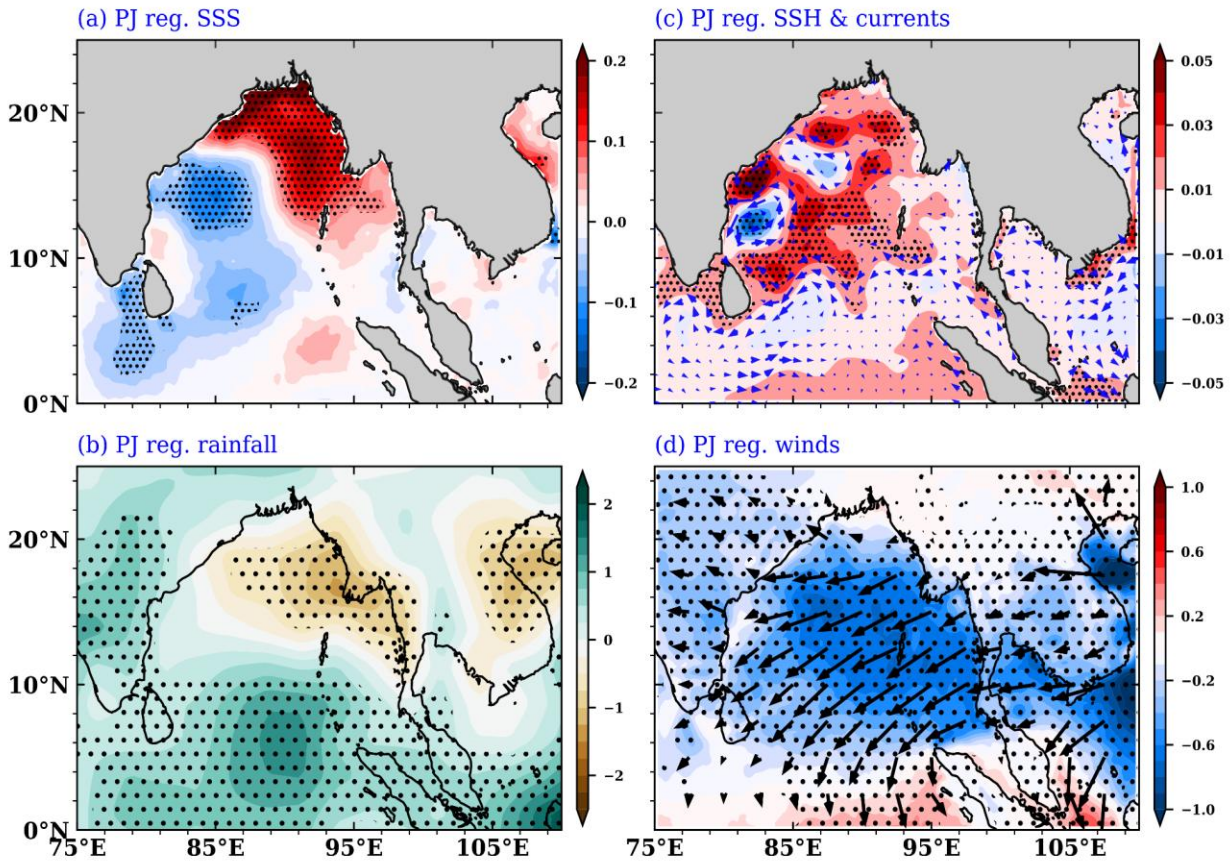

Figure 3. Regression of the standardized PJ index onto JJA-mean anomalies of (**a**), sea surface salinity (SSS); (**b**), sea surface height (SSH; shading, m) and surface currents (vectors, m s^{-1}); (**c**), precipitation (mm day^{-1}); and (**d**), surface winds (m s^{-1}). Stippling indicates regression coefficients statistically significant at the 95% confidence level.

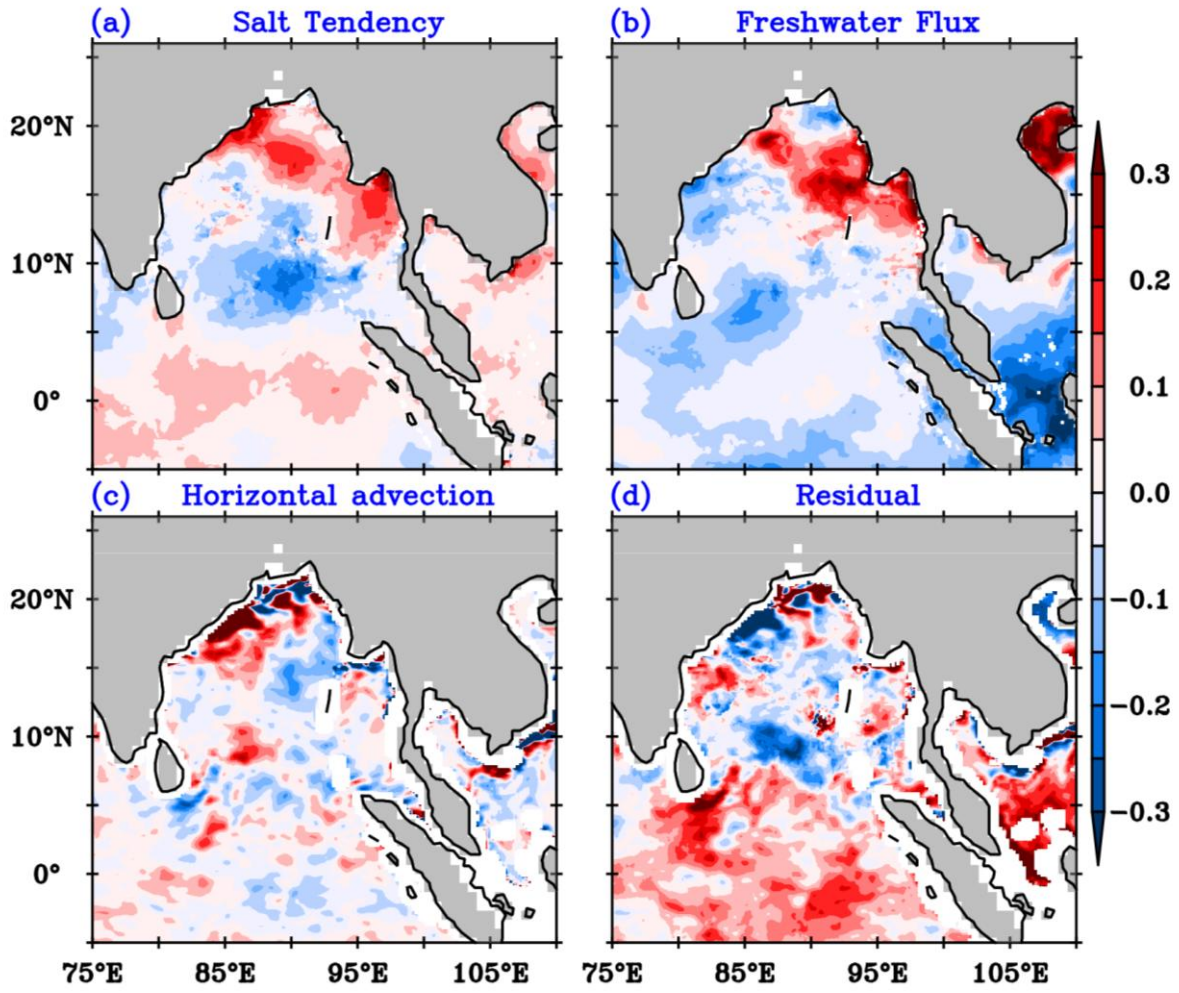

Figure 4. Regression of the standardized PJ index onto JJA-mean mixed-layer salinity budget terms: (**a**), salinity tendency; (**b**), surface freshwater forcing; (**c**), horizontal advection; and (**d**), residual. Mixed-layer salinity and mixed-layer depth are derived from the Copernicus multi-observation three-dimensional ocean product, ocean currents from ORAS5, and precipitation and evaporation from ERA5. See Methods for the mixed-layer salinity budget formulation.

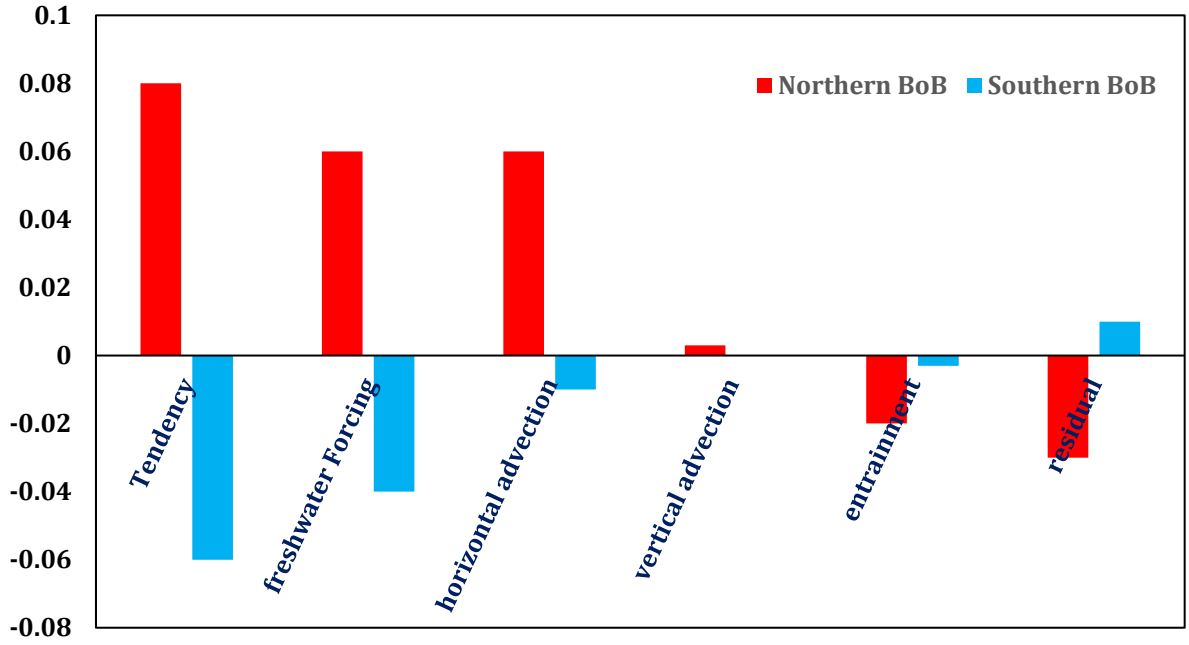

Figure 5. Area-averaged regression of mixed-layer salinity budget terms onto the standardized PJ index over the northern (red) and southern (blue) Bay of Bengal (BoB). Terms include mixed-layer salinity tendency, surface freshwater forcing, horizontal advection, vertical advection, entrainment, and residual. Positive (negative) values indicate processes contributing to salinification (freshening) during the positive PJ phase. Regression coefficients are expressed per standard deviation of the PJ index.

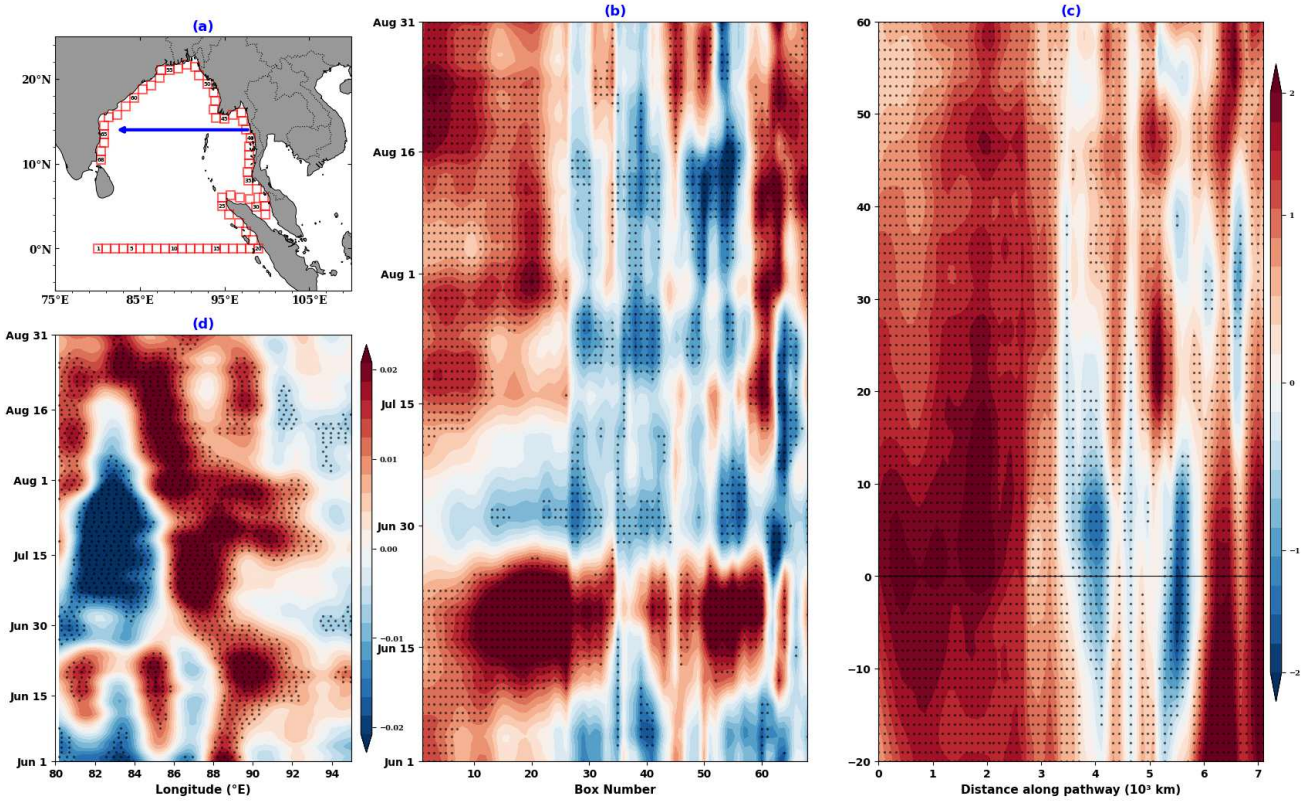

Figure 6. (a) Pathways used to diagnose equatorial and coastal Kelvin waves and interior Rossby waves. Numbered 1° × 1° boxes in define the sequential averaging regions along the Kelvin-wave pathway, while the transect at 14°N defines the Rossby-wave pathway. **(b)**, Hovmöller diagram of PJ-regressed daily sea-level anomaly (SLA) along the Kelvin-wave pathway. **(c)**, Lagged regression of SLA onto the PJ index as a function of cumulative distance along the Kelvin-wave pathway; positive lag denotes PJ leading SLA. **(d)**, Longitude–time Hovmöller diagram of PJ-regressed SLA along 14°N. Stippling indicates statistical significance at the 95% confidence level. Regression coefficients are expressed per standard deviation of the PJ index.

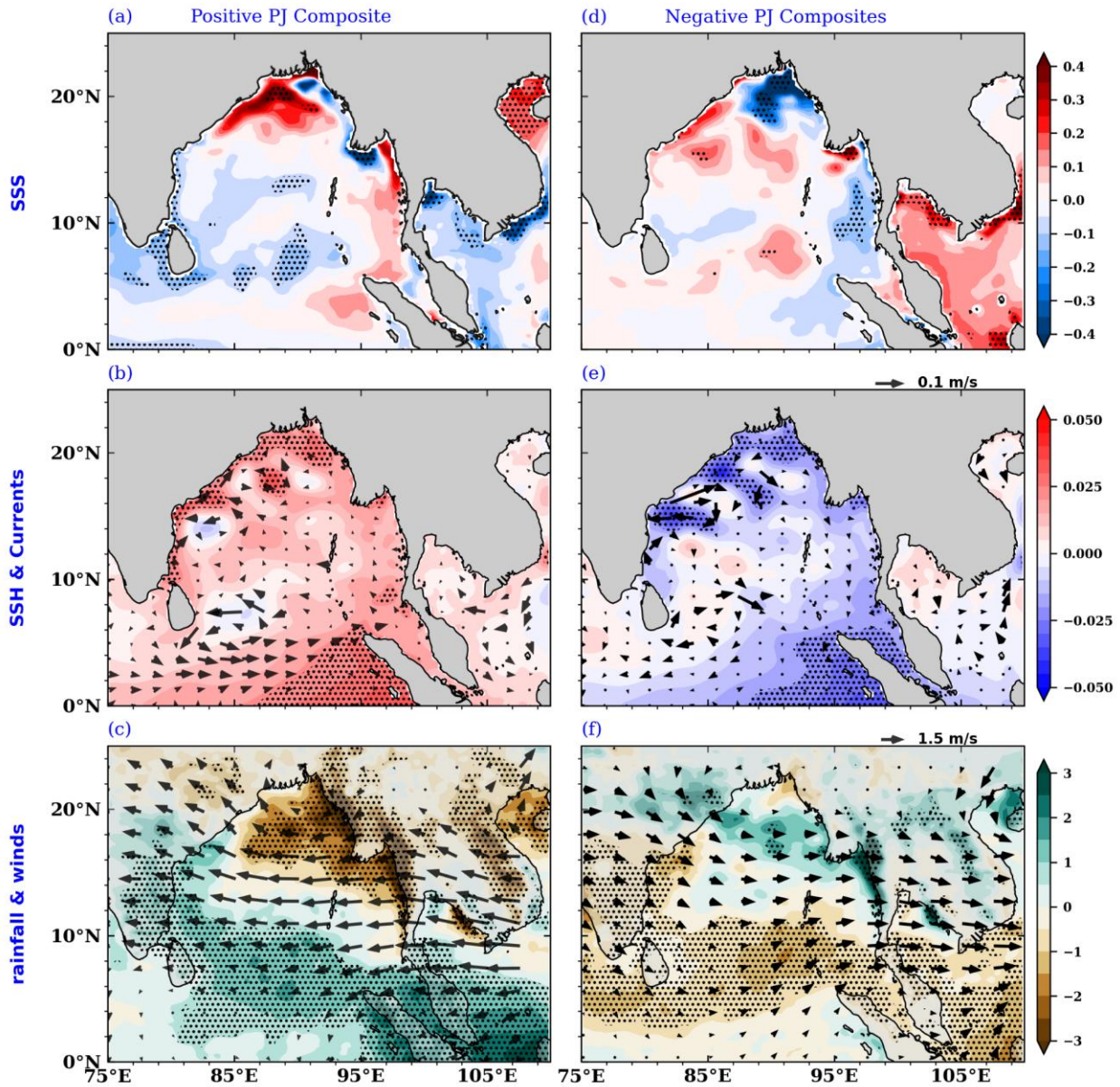

Figure 7. Average JJA composites of **(a)** SSS (shaded), **(b)** SSH (shaded, m) and surface currents (vectors, m/s), and **(c)** rainfall (shaded, mm/day) and surface winds (vectors, m/s) during the positive PJ years. **(d) - (f)** same as (a) - (c) but for the composites of negative PJ years. The composite analysis is carried out from ORAs5 during the period 1980 – 2025. Stippling indicates the statistical significance at 95% confidence level.

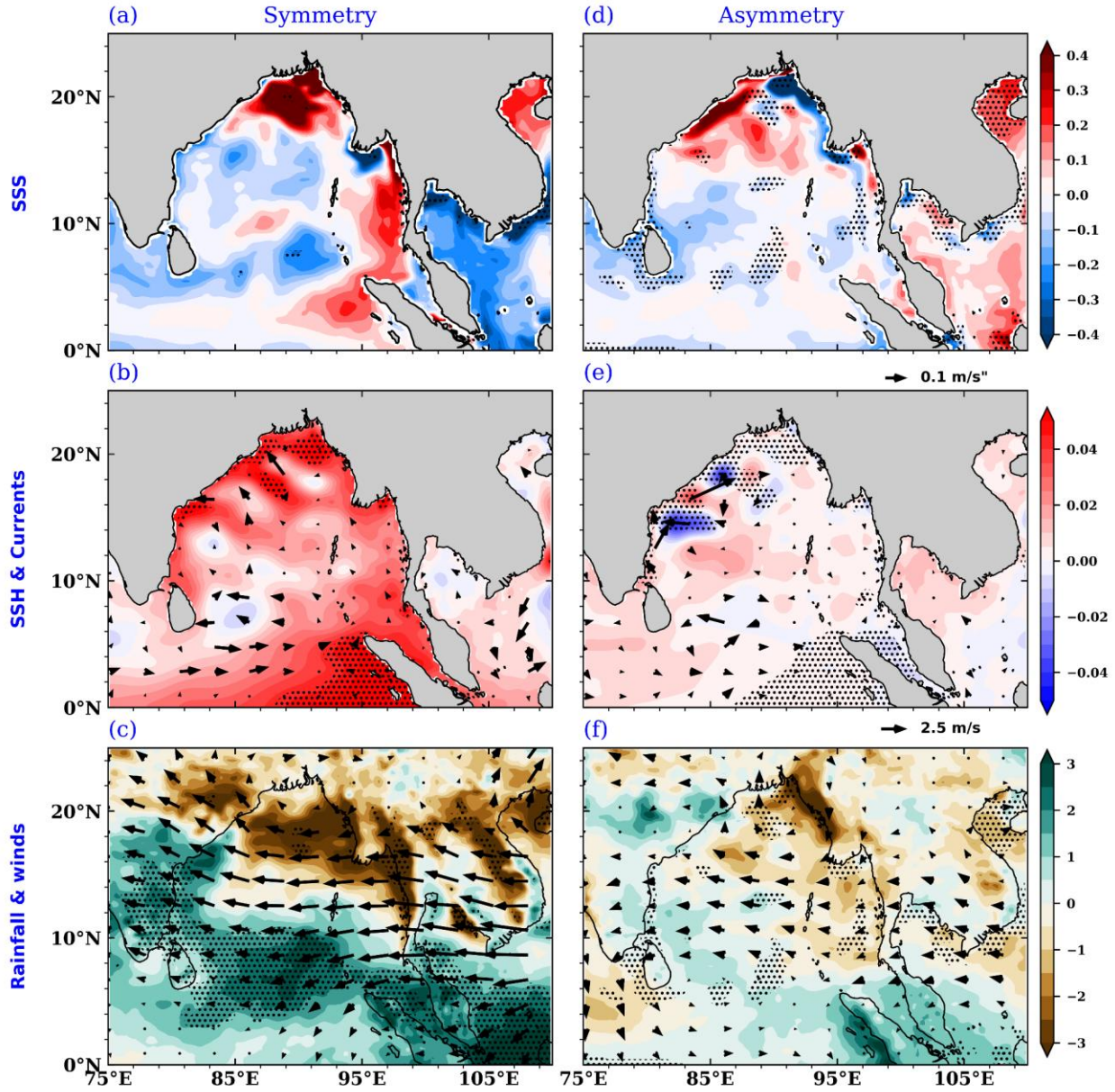

Figure 8. Average JJA composite of symmetrical (obtained as (positive PJ – negative PJ) and asymmetrical (obtained as positive PJ + negative PJ) anomalies for **(a)**, **(d)** SSS (shaded), **(b), (e)** SSH (shaded, m) and surface currents (vectors, m/s), and **(c), (f)** rainfall (shaded, mm/day) and surface winds (vectors, m/s). Stippling indicates the statistical significance at 95% confidence level.

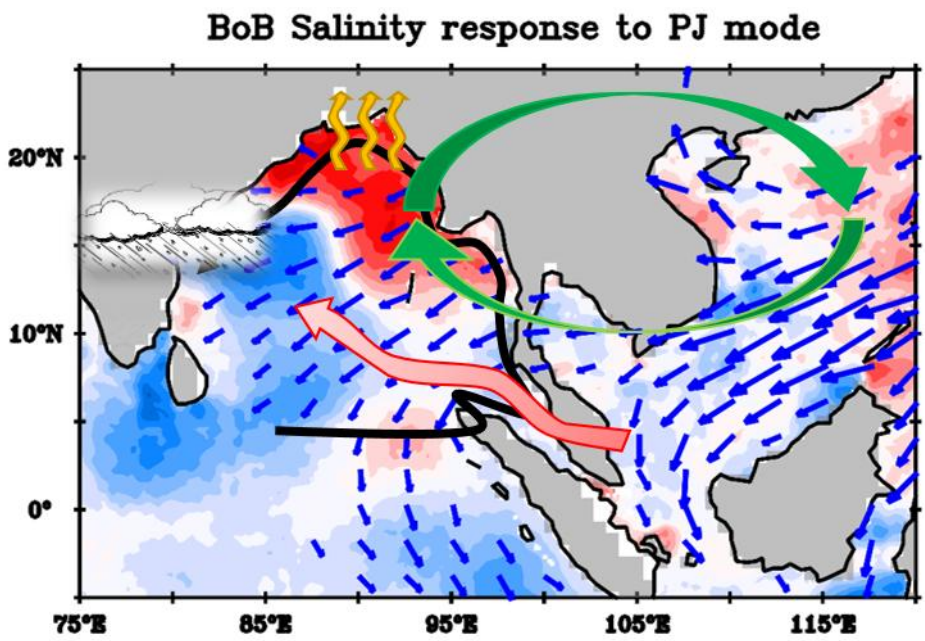

Figure 9. Schematic representation of the salinity response over the Bay of Bengal to the PJ pattern. Color shading represents sea surface salinity, and blue vectors denote surface wind anomalies. The green elliptical arrows indicate the anomalous anticyclonic circulation over the western North Pacific, while the red ribbon arrow represents the westward propagation of Rossby waves. The black contour along the coast denotes the propagation pathway of coastal Kelvin waves. Upward yellow arrows indicate enhanced evaporation over the northern Bay of Bengal, whereas the clouds over the Indian landmass and southern Bay of Bengal indicate enhanced precipitation.